Corrosion Science 249 (2025) 112869

Contents lists available at ScienceDirect

Corrosion Science

journal homepage: www.elsevier.com/locate/corsci

Effect of $MgSO_4$ addition on alkali sulphates induced hot corrosion of a β-NiAl coating

Yaping Wang [a], Egbert Wessel [a], Daniel Grüner [a], Rishi Pillai [a,1], Elena Yazhenskikh [a], Martin Frommherz [b], Michael Müller [a], Willem Joseph Quadakkers [a], Dmitry Naumenko [a,*]

[a] Forschungszentrum Jülich GmbH, Institute of Energy and Climate Research (IEK-2), Wilhelm-Johnen-Straße, Jülich 52428, Germany
[b] MTU Aero Engines AG, Dachauer Strasse 665, München 80995, Germany

ARTICLE INFO

Keywords:
Molten salts (A)
Metal coatings (A)
SEM (B)
Hot corrosion (C)
Thermodynamic diagrams (C)

ABSTRACT

The effect of $MgSO_4$ addition on alkali sulphates induced hot corrosion of a β-NiAl coating was studied by performing a series of tests with deposits of Na_2SO_4, Na_2SO_4-20 %K_2SO_4 and Na_2SO_4-12 %K_2SO_4-35 %$MgSO_4$ (mol.% for all) at 700 °C in air with addition of SO_2. For elucidating the observed corrosion phenomena, various salt-oxide/NiAl powder mixtures were exposed to the same hot corrosion test conditions. Two pseudo-binary phase diagrams of the Na, K, Mg-sulphate systems were calculated using an in-house developed thermodynamic database. Addition of $MgSO_4$ to Na_2SO_4-20 %K_2SO_4 deposit salt inhibited the hot corrosion attack during 24 h exposure, which is related to consumption of aggressive K_2SO_4 by the formation of solid $K_2Mg_2(SO_4)_3$. However, extending the exposure with Na_2SO_4-12 %K_2SO_4-35 %$MgSO_4$ deposit to 100 h resulted in severe corrosion attack. The latter observation is explained by a reaction between $K_2Mg_2(SO_4)_3$ and NiAl causing formation of a Mg, Ni and Al containing spinel accompanied by release of the aggressive K_2SO_4 into the liquid phase.

1. Introduction

Hot corrosion is an accelerated reaction of alloys and coatings induced by deposits of sulphate salts at elevated temperatures [1,2]. These sulphate salts usually have the following sources in a marine gas turbine engine: (1) sulphur is commonly incorporated from the residual of the combustion fuel or the air pollution; (2) alkali and alkaline earth oxides are ingested in the intake air. During the last decades, various studies were carried out to understand the relevant corrosion reactions and mechanisms [3–9]. Most of the conventional hot corrosion investigations were performed using Na_2SO_4 as deposit [3,4,10]. At temperatures around 700 °C the classical mechanism of hot corrosion is the so-called type II, i.e. Na_2SO_4 forms a liquid eutectic by reacting with $NiSO_4$, the latter being produced by a reaction of Ni with SO_3 present in the operation environment.

In practice, other sulphates are commonly identified on the surface of turbine components apart from Na_2SO_4 [11–14]. As shown in Table 1, $MgSO_4$, $CaSO_4$, and K_2SO_4 are frequently observed on surfaces of turbine blades.

The mechanisms of hot corrosion induced by various sulphates and especially by their mixtures have not been extensively studied. Regarding alkali sulphates, it was shown in our previous investigation that addition of K_2SO_4 to the Na_2SO_4 base deposit can significantly accelerate the corrosion attack. It was proposed that the presence of K_2SO_4 lowers the temperature of the eutectic reaction in the ternary system Na_2SO_4-K_2SO_4-$NiSO_4$ and/or pSO_3 required to stabilize the liquid phase [33].

Several studies are available on the effect of alkaline-earth sulphate additions to alkali sulphate based deposit in hot corrosion of high-temperature alloys. Rahmel et al. [16] reported that addition of $MgSO_4$ and $CaSO_4$ into alkali sulphates considerably decreased the corrosion rate of a Cr and Ni containing stainless steel at 650 °C. It was proposed that formation of thermodynamically stable compounds - $K_2Mg_2(SO_4)_3$ (melting temperature: 930 °C [17–19]) and $K_2Ca_2(SO_4)_3$ (melting temperature: 1011 °C [20]) prevented a rapid corrosion reaction of the steel. Jones et al. [21] found that the corrosion rate of a Co-based alloy was significantly lower in a deposit containing $MgSO_4$--Na_2SO_4 than that in a deposit containing only Na_2SO_4 at 700 °C during

* Corresponding author.
E-mail address: d.naumenko@fz-juelich.de (D. Naumenko).
[1] Oak Ridge National Laboratory, Materials Science and Technology Division, Oak Ridge, Tennessee, 37831, USA (present address)

https://doi.org/10.1016/j.corsci.2025.112869
Received 13 October 2023; Received in revised form 6 September 2024; Accepted 13 March 2025
Available online 17 March 2025

Table 1
Salt composition found on turbine blade surfaces [15].

Airfoil Surface	Salt Constituent	First Stage Deposit Chemistry (mole %)	Second Stage Deposit Chemistry (mole %)
External (gas path)	Na_2SO_4	40	28
	K_2SO_4	4	3
	$CaSO_4$	40	59
	$MgSO_4$	13	8
Internal (cooling passages)	Na_2SO_4	45	37
	K_2SO_4	3.2	4.4
	$CaSO_4$	41	46
	$MgSO_4$	9.5	11.5

24 h exposure. It was proposed that the presence of $MgSO_4$ reduced the corrosion rate by inhibiting the Co_3O_4 sulphation/dissolution process. In contrast to [16] and [21] a negative effect of $MgSO_4$-addition to a Na_2SO_4 based deposit on the hot corrosion attack of model and commercial Ni-base superalloys was observed by Galetz and co-workers [22,23]. A more severe corrosion attack under the deposit of the Na_2SO_4-$MgSO_4$ eutectic mixture compared to that under the Na_2SO_4 deposit in an atmosphere with high SO_2 contents (0.1 % SO_2 and 0.5 % SO_2) at 700 °C [22,23] was attributed to the low melting temperature of the eutectic salt mixture.

Aim of the present study is the elucidation of the effect of $MgSO_4$ addition on the hot corrosion behaviour of a beta-NiAl coating beneath a Na/K-sulphate deposit. For this purpose, a beta-NiAl coated single crystal Ni-based superalloy was exposed in ternary Na_2SO_4-K_2SO_4-$MgSO_4$ deposit in air containing SO_2. To understand the complex reactions within the salt and between the salt and the coating elements, various powder mixtures of Na_2SO_4-K_2SO_4-$MgSO_4$ and NiO/NiAl were prepared and exposed under the same test conditions as those used for the corrosion testing of the coating systems. The experimental studies were supported by thermodynamic equilibria calculations using FACTSAGE and an extensive in-house developed sulfate database [24–26]. Based on the obtained experimental and modelling results, the effect of $MgSO_4$ addition on alkali sulphate induced hot corrosion is extensively discussed. For easier readability of the manuscript, the results will be compared with few, selected data from reference [33] in which the corrosion behaviour in single and binary K- and Na-sulphates was extensively investigated.

2. Materials and methods

2.1. Materials

A β-NiAl diffusion coating on the 2nd generation Ni-based single-crystal superalloy with a composition Ni-9.91Co-4.85Cr-5.63Al-9Ta-6W-2Mo-3Re-0.1Hf (wt%). was employed in the present work. The coating was manufactured using an industrial chemical vapour deposition (CVD) process with a low Al activity. The thickness of the coating is approximately 60 μm. Concerning its morphology, this β-NiAl coating can be divided into two parts, which are usually designated as the outer coating and the interdiffusion zone, as shown in our previous work [27]. The outer coating is of great importance for the present study and consists of a β-NiAl phase with the composition of around Ni-41Al-6Co-2Cr (at%). The thickness of the outer coating is approximately 30 μm.

2.2. Experimental methods

2.2.1. Hot corrosion tests

Na_2SO_4-$12K_2SO_4$-$35MgSO_4$ (mol.%) was selected as the deposits for the hot corrosion tests in the present study. This composition has the lowest melting temperatures in the corresponding ternary system [24,25,28,29]. Tests with Na_2SO_4 and Na_2SO_4-$20K_2SO_4$ were performed in our previous work using an identical procedure [33] and the respective selected data of post-exposure analytics are shown in the section "Results" below as reference to elucidate the effect of $MgSO_4$ addition. For preparing the deposits, 82 wt% dry salt powder was mixed with a solvent consisting of 95 wt% terpineol and 5 wt% ethyl cellulose to produce a deposit slurry. 20 × 10 × 2 mm^3 rectangular coupon specimens of the studied coated Ni-based superalloy were used for all hot corrosion tests. The slurry was painted onto one surface of the specimens. Prior to the corrosion tests, the specimens were dried at 60 °C for 12 h. Assuming all terpineol evaporated during drying, the final composition of the deposit was the designed salt mixture with around 1 wt% cellulose. The amount of deposit on the sample surface after drying was measured to be approximately 30 mg/cm^2.

In addition to the coated Ni-base alloys, corrosion tests were performed with NiO or NiAl powders (each of 99.95 % purity) mixed with respective sulphates. The latter tests allowed an easier elucidation of the corrosion mechanisms because effects of alloying elements in the NiAl-coating such as Co or Cr could be eliminated. Moreover, homogeneous reaction morphologies could be obtained with the powder mixtures that substantially facilitated analysis of the corrosion products.

The coated specimens with the salt deposits and powder mixtures were laid into alumina crucibles and put into a horizontally arranged tube furnace for the tests. The test gas was synthetic air with 300 or 1000 ppm SO_2. A platinum honeycomb was placed in front of the specimens in the furnace to catalyse the reaction between O_2 and SO_2 for producing SO_3, which ensured the equilibrium gas composition during the tests [30,31]. The exposure temperature was 700 °C and the duration was 24 h or 100 h. The heating and cooling rate were 10 °C/min and 2 °C/min, respectively.

2.2.2. Metallographic analysis

Polished metallographic cross-sections of the specimens and powder mixtures after exposure were prepared using a water-free procedure to preserve any water-soluble species. The morphologies of the corrosion attack were observed using scanning electron microscopy (SEM) using Merlin and Supra 50 VP field emission microscopes (Zeiss, Oberkochen, Germany). The elemental distribution in the salt, the corrosion products and the coated alloy was analysed by energy dispersive X-ray (EDX) microanalysis using X-max silicon drift detectors (Oxford Instruments, High Wycombe, UK).

2.2.3. X-ray diffraction (XRD)

XRD measurements were performed for the phase identification of the Na_2SO_4-$12K_2SO_4$-$35MgSO_4$ mixture using an Empyrean diffractometer (Malvern Panalytical) with Cu-K_α radiation (40 kV, 40 mA) and a PIXcel3D detector. The inorganic crystal structure database (ICSD, FIZ Karlsruhe) [32] was used for the evaluation of the obtained XRD patterns.

3. Experimental results

3.1. Hot corrosion morphologies after 24 h exposure

Hot corrosion tests without deposits, with Na_2SO_4, Na_2SO_4-$20K_2SO_4$ and Na_2SO_4-$12K_2SO_4$-$35MgSO_4$ mixtures on top of the studied β-NiAl coating were performed at 700 °C for 24 h. As shown in Fig. 1a, no significant corrosion attack was found in the salt-free specimen. For the specimen with Na_2SO_4 deposit, discontinuous pits were observed (Fig. 1b). The exposure with Na_2SO_4-$20K_2SO_4$ resulted in the formation of a thick multiphase corrosion layer and an Al-depleted zone beneath it (Fig. 1c). However, no visible corrosion attack was found in the specimen beneath Na_2SO_4-$12K_2SO_4$-$35MgSO_4$, and a thick dense deposit layer was observed on top of the specimen (Fig. 1d). Apparently, the hot corrosion reaction induced by alkali sulphates, especially the Na_2SO_4-$20K_2SO_4$ was inhibited by the addition of $MgSO_4$ during the 24 h exposure. Results from Fig. 1(a) and (b) were reported in our previous work [33] and are shown here as reference to better illustrate the effect

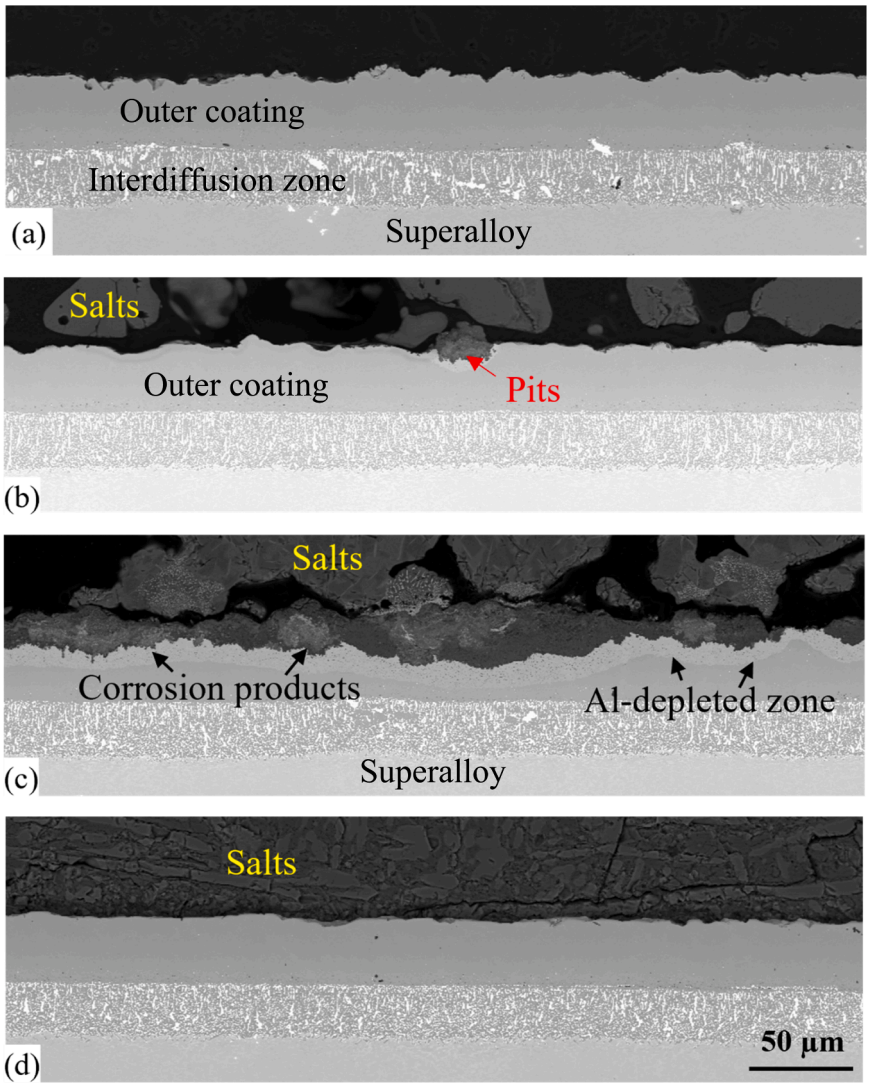

Fig. 1. SEM-BSE images of the cross-sections of studied β-NiAl coating on Ni-based superalloy after hot-corrosion testing at 700 °C for 24 h in air-300 ppm SO_2 (a) without deposits [33], (b) with Na_2SO_4 [33], (c) with Na_2SO_4-$20K_2SO_4$ (d) with Na_2SO_4-$12K_2SO_4$-$35MgSO_4$ deposits.

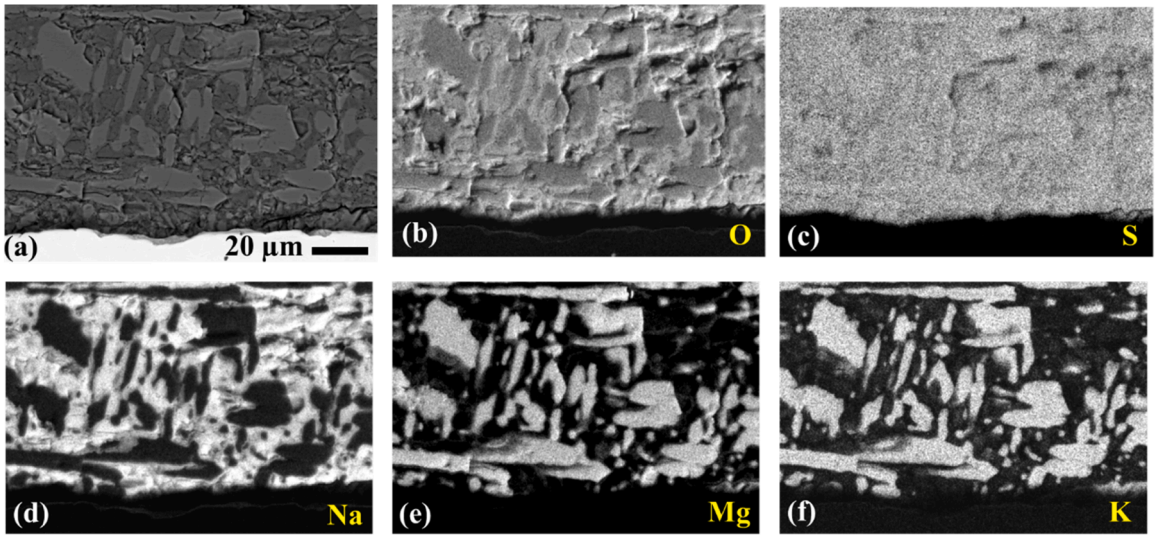

Fig. 2. (a) SEM-BSE image and (b)-(f) corresponding EDX-elemental maps of the cross-section of studied β-NiAl coating on Ni-based superalloy after hot-corrosion testing with Na_2SO_4-$12K_2SO_4$-$35MgSO_4$ at 700 °C for 24 h in air-300 ppm SO_2.

of Mg-sulfate addition.

The EDX maps of the Na_2SO_4-$12K_2SO_4$-$35MgSO_4$ mixture on top of the NiAl coated specimen after 24 h exposure are shown in Fig. 2. O and S were distributed homogeneously throughout the mixture; Mg and K overlapped at some locations where Na was absent, indicating the formation of a mixed Mg, K-sulphate phase during exposure.

According to our previous study [33], a sufficiently high partial pressure of SO_3 in the atmosphere is essential to produce the liquid phase, and thereby to cause severe hot corrosion attack during the exposure of coated Ni-base superalloy under alkali sulphates at 700 °C. To study the effect of the partial pressure of SO_3 on Na, K, and Mg-sulphate mixture induced hot corrosion, the NiAl coating beneath the Na_2SO_4-$12K_2SO_4$-$35MgSO_4$ mixture was exposed to air-1000 ppm SO_2 for 24 h. Substantial frontal attack was found at the interface between the salt and the coating after exposure (Fig. 3a). Clearly, increasing the SO_2 content in the atmosphere accelerated the attack (compare with Fig. 1d).

The BSE-image and the corresponding EDX-elemental maps of the selected area marked by the red dashed frame in Fig. 3a are shown in Fig. 3b-i. Mg and K are found in the same locations, and Na distributed elsewhere above the corrosion products, which is similar to the salt morphology after exposure to air-300 ppm SO_2 (compare with Fig. 2). Al-rich oxides were identified as the predominant corrosion products. Mg, Ni and S were also detected in the corrosion layer apart from Al and O, indicating the existence of mixed Mg/Al- and Ni/Al-oxides, probably $MgAl_2O_4$, $NiAl_2O_4$ spinel phases as well as Ni-sulphate and/or Ni-sulphide. Ni-sulphide precipitates were found on top and in the inner part of the corrosion layer as marked by the red arrows. Ni-oxide was observed on top of the corrosion layer as marked by the green arrows. Co-oxide and sulphide were also identified (Fig. 3i).

3.2. Hot corrosion morphologies after 100 h exposure

The corrosion morphology of the studied NiAl coating after exposure under Na_2SO_4-$20K_2SO_4$ and Na_2SO_4-$12K_2SO_4$-$35MgSO_4$ mixtures at 700 °C in air-300 ppm SO_2 for 100 h is shown in Fig. 4. A severe corrosion attack occurred in both cases and the attack depths are comparable. Comparison of this finding with the 24 h results shown in Fig. 1 and Fig. 2 shows that the addition of $MgSO_4$ into alkali sulphates extended the incubation time for hot corrosion but did not inhibit the attack during longer time exposure up to 100 h. Intermediate sulphate compounds: $(Na, K)_2(Ni, Co)(SO_4)_2$ are identified in the Na_2SO_4-$20K_2SO_4$ deposit after 100 h exposure at 700 °C in air-300 ppm SO_2, as shown in Fig. 5. The corrosion products and their morphology in the specimen with Na_2SO_4-$20K_2SO_4$ were described in detail in our previous work [33] and will therefore not be repeated here.

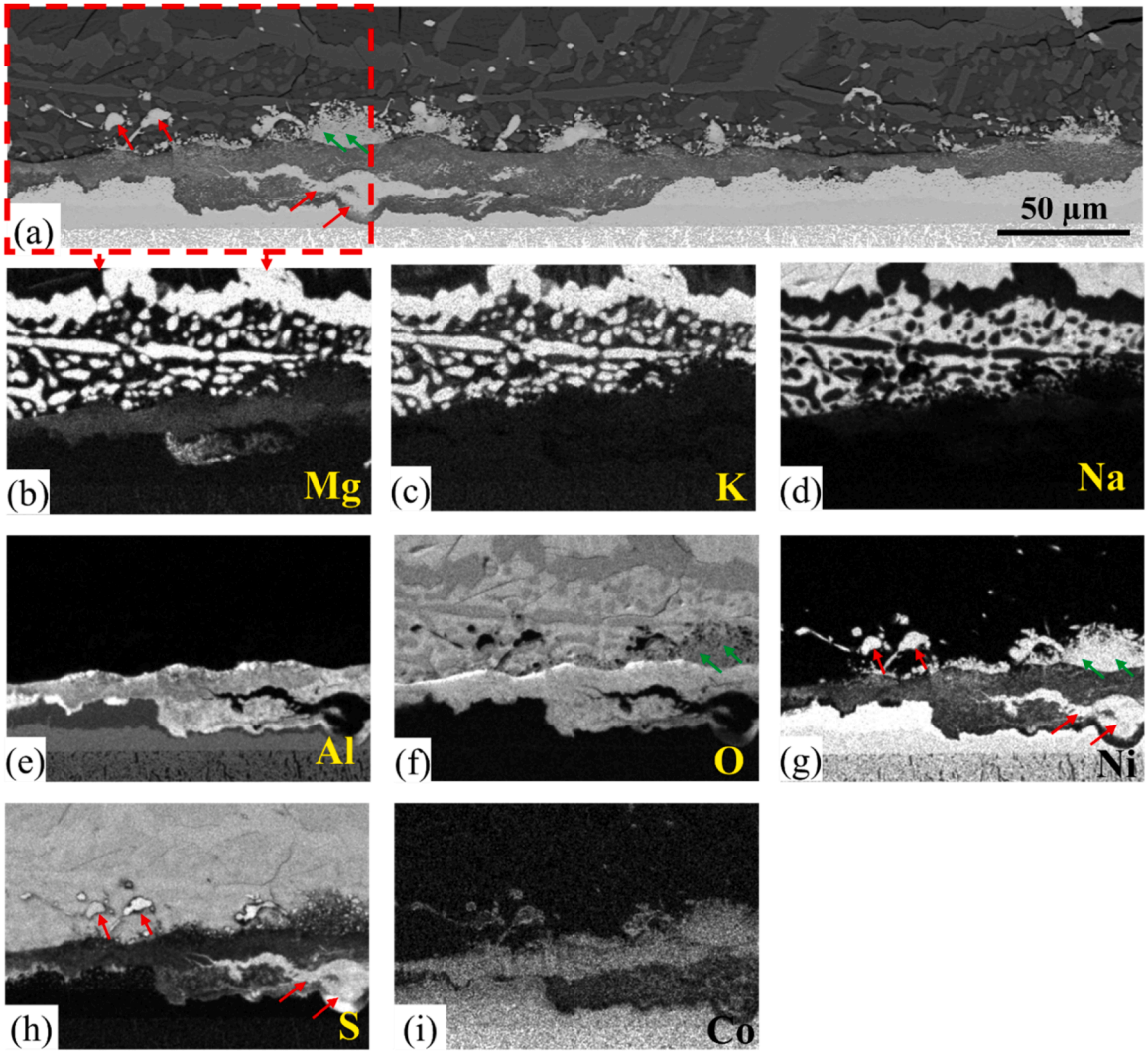

Fig. 3. (a) SEM-BSE image and (b)-(i) corresponding EDX-elemental maps of the selected area marked by the red frame in (a) in the cross-section of studied β-NiAl coating on Ni-based superalloy after hot-corrosion testing with Na_2SO_4-$12K_2SO_4$-$35MgSO_4$ deposit at 700 °C for 24 h in air-1000 ppm SO_2. The phases marked by the red and green arrows are Ni-sulphide and Ni-oxide precipitates, respectively.

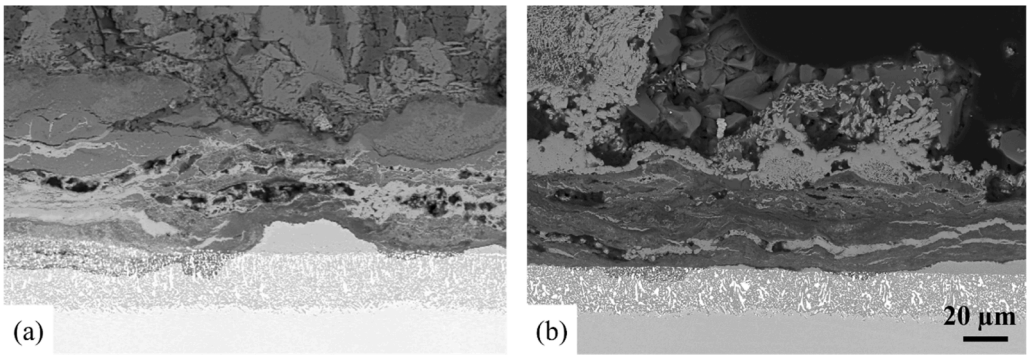

Fig. 4. SEM-BSE images of the cross-sections of studied β-NiAl coating on Ni-based superalloy after hot-corrosion testing at 700 °C for 100 h in air-300 ppm SO_2 with (a) Na_2SO_4-20K_2SO_4 (b) Na_2SO_4-12K_2SO_4-35$MgSO_4$.

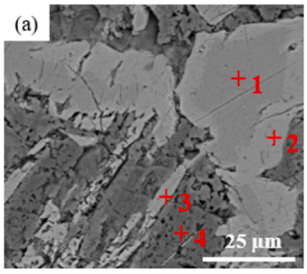

(b)	O	S	Na	K	Ni	Co	Phase
1	61.7	15.6	12.6	2.9	5.7	1.6	$(Na, K)_2(Ni, Co)(SO_4)_2$
2	61.4	15.4	7.4	8.4	5.6	1.8	ternary sulphate Na:K:(Ni,Co) ≈ 1:1:1
3	61.5	15.5	6.7	9.4	4.5	2.5	
4	57.5	14.4	26.8	0.9	0.4	0.0	Na_2SO_4 s.s.

Fig. 5. (a) SEM-BSE image of cross-section of studied β-NiAl coating on Ni-base superalloy after hot-corrosion testing with Na_2SO_4-20K_2SO_4 at 700 °C in air-300 ppm SO_2 for 100 h, (b) corresponding EDX point analyses of element concentrations (at%) of zones 1–4 in (a) [33].

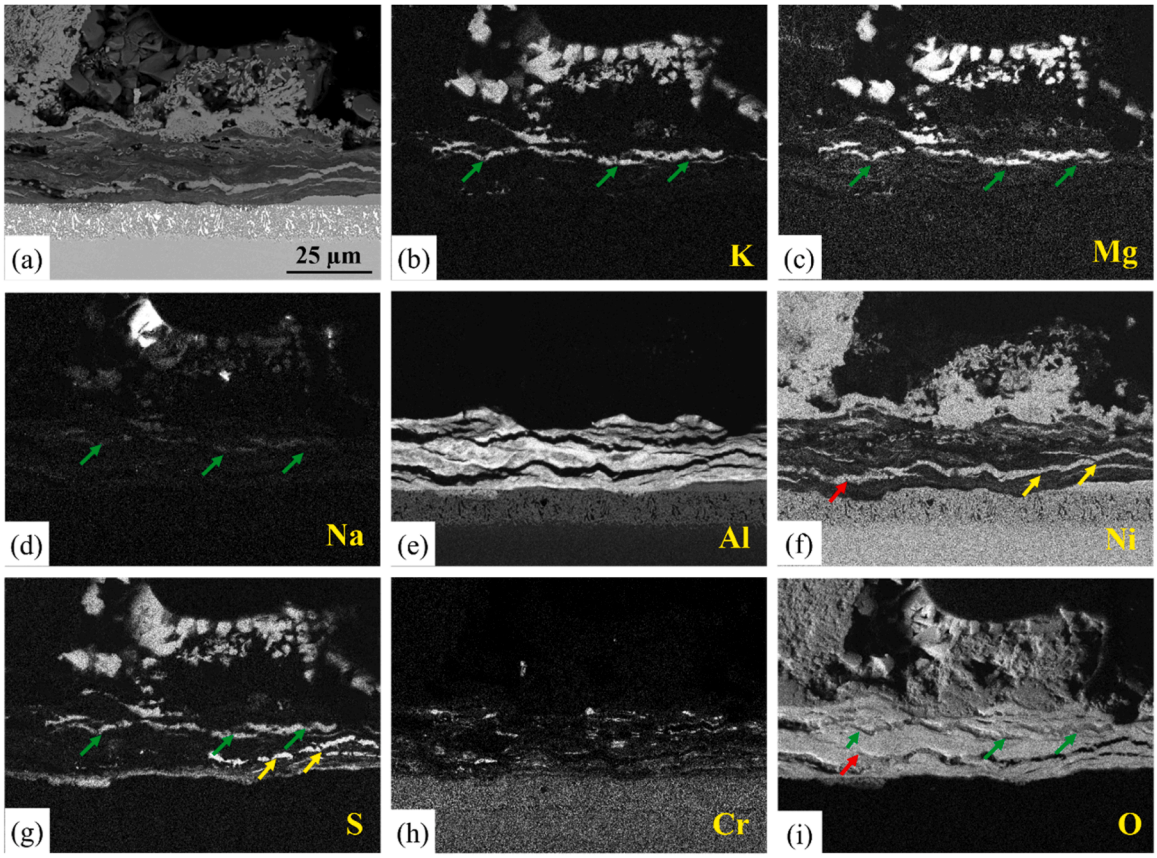

Fig. 6. (a) SEM-BSE image and (b)-(i) corresponding EDX-elemental maps of the cross-section of the studied β-NiAl coating on Ni-base superalloy after hot-corrosion testing with Na_2SO_4-12K_2SO_4-35$MgSO_4$ at 700 °C for 100 h in air-300 ppm SO_2. The phases marked by the green arrows are a mixture of K, Mg, Na-sulphate phases. The phases marked by the red and yellow arrows are Ni oxide and sulphide precipitates, respectively.

The elemental distribution of the studied NiAl coating with Na_2SO_4-$12K_2SO_4$-$35MgSO_4$ mixture after 100 h exposure at 700 °C for 100 h in air-300 ppm SO_2 is shown in Fig. 6. Overlapping of K, Mg, S and O maps in the deposit as well as in the upper part of the corroded coating (green arrows in Fig. 6), indicate the existence of a K, Mg mixed sulphate compound. The Al-rich oxide layer intermixed by the salts and the precipitation of Ni oxides / sulphides (yellow arrows in Fig. 6) were recognized as the main corrosion products, which is qualitatively similar to those identified in the specimen with the Na_2SO_4-$20K_2SO_4$ deposit [33]. Careful analysis of the Mg map indicates that some Mg is also present in the Al-rich oxide layer.

3.3. Exposure of powder mixtures of sulphate salt and NiO/NiAl

For obtaining a more detailed understanding of the reactions within the Na_2SO_4-$12K_2SO_4$-$35MgSO_4$ mixture, XRD analysis was performed after the exposure of the ternary powder mixture (i.e. without presence of a NiAl coated specimen) at 700 °C in air-300 ppm SO_2 for 24 h, and the corresponding result is shown in Fig. 7. A langbeinite phase $K_2Mg_2(SO_4)_3$ and a $(Na, K)_2SO_4$ phase were identified apart from Na_2SO_4. $(Na, K)_2SO_4$ corresponds to the glaserite solid solution phase in the Na_2SO_4-K_2SO_4 system [25]. A quantification of the XRD pattern shows that the mixture consists of approximately 87 mol. % Na_2SO_4, 3 mol. % $(Na, K)_2SO_4$ and 10 mol. % $K_2Mg_2(SO_4)_3$. Some additional minor peaks can be seen in Fig. 7, which could not be reliably identified due to their low intensity. These peaks might belong to mixed NaMg-mixed sulphates, as indicated by thermodynamic calculations presented in Section 4 below.

To study the morphology evolution of the ternary sulphate salt and reactions between the salt and NiO during exposure, NiO was added to the Na_2SO_4-$12K_2SO_4$-$35MgSO_4$ mixture to produce a salt-oxide mixture with the composition of Na_2SO_4-$7K_2SO_4$-$22MgSO_4$-38NiO (mol.%). The amount of NiO added was adjusted to our previous study [33] with Na and Na/K-mixed sulphates in order to keep NiO to sulphate ratio constant. This salt-oxide mixture was exposed to 700 °C in air-300 ppm SO_2 for 100 h. The morphology and the elemental distributions after exposure are shown in Fig. 8. According to the EDX-maps in Fig. 8c-h and point analysis results in Table 2, $K_2Mg_2(SO_4)_3$ (spectrum 1) and Na_2SO_4 (spectrum 2) were identified. Approximately 1.6 and 0.8 at% Ni was detected in the $K_2Mg_2(SO_4)_3$ and Na_2SO_4, respectively. Minor amounts of the salt cations and sulphur were also detected in the NiO particles (spectrum 3 in Table 2).

To study the reaction between the ternary salt mixture and NiAl powder, a Na_2SO_4-$7K_2SO_4$-$22MgSO_4$-38NiAl mixture (Na_2SO_4-$12K_2SO_4$-$35MgSO_4$ with addition of 38 mol.% NiAl powder) was prepared and exposed at 700 °C in air-300 ppm SO_2 for 100 h. The morphology and elemental distributions after exposure are shown in Fig. 9. The NiAl powder and the salt reacted as shown in Fig. 9a. The reaction products are mainly Al-rich oxides (compare Fig. 9e and g), and Ni-rich oxides and sulphides (compare Fig. 9f, g and h). Na, K, and Mg are also found in the Al and Ni reacted zone (the left part of Fig. 9a). At locations where no Ni or Al involved reactions are found (the upper right part of Fig. 9a), precipitates of the mixed Mg, K sulphate phase ($K_2Mg_2(SO_4)_3$) dispersed in a Na_2SO_4-rich phase containing some K are observed.

Fig. 10 shows an XRD-pattern collected from the reacted Na_2SO_4-$7K_2SO_4$-$22MgSO_4$-38NiAl powder mixture. Apart from the two major deposit constituents (Na_2SO_4 and $K_2Mg_2(SO_4)_3$) a number of corrosion products were identified. The latter included NiO and Ni_3S_2 as well as Al_2O_3 and a spinel phase ($MgAl_2O_4$). The results of the XRD-studies are in very good agreement with the corresponding SEM/EDX results (compare Fig. 9 and Fig. 10).

4. Thermodynamics of the Na_2SO_4-K_2SO_4-$MgSO_4$ system

A sulphate thermodynamic database containing the Na_2SO_4-K_2SO_4-$MgSO_4$ system and the corresponding sub-systems was developed and recently optimized by Yazhenskikh et al. [24,25]. To understand the phase equilibria in the complex Na, K, Mg-ternary sulphate system, the phase diagram of a pseudo-binary system $(MgSO_4)_{0.88}(K_2SO_4)_{0.12}$-$(Na_2SO_4)_{0.88}(K_2SO_4)_{0.12}$ based on the ternary sulphate system were calculated in FactSage 7.3 [34] using the optimized database, and the corresponding result is shown in Fig. 11a. The pseudo-binary system $(MgSO_4)_{0.88}(K_2SO_4)_{0.12}$-$(Na_2SO_4)_{0.88}(K_2SO_4)_{0.12}$ was chosen because of the eutectic composition Na_2SO_4-$12K_2SO_4$-$35MgSO_4$ reported for the ternary system [24]. The latter composition of the ternary sulphate deposit was used for hot corrosion tests in the present work. The eutectic point is marked by the red point in Fig. 11a. The compound $K_2Mg_2(SO_4)_3$ was identified both on the surface of the NiAl specimen beneath the deposit after exposure (Fig. 2), in the sulphate salt powder mixture (Fig. 7) and the salt-NiO/NiAl mixtures (Figs. 8–10 and Table 2) after exposure. To understand the reactions between $K_2Mg_2(SO_4)_3$ and Na_2SO_4, the phase diagram of the $K_2Mg_2(SO_4)_3$-Na_2SO_4 pseudo-binary system was also calculated, and the corresponding result is shown in Fig. 11b. As shown in Fig. 11a, the Na_2SO_4-$12K_2SO_4$-$35MgSO_4$ mixture appears at 700 °C in the equilibrium condition in a liquid form and solidifies to form a Na_2SO_4 based solid solution phase HEXA [25,35] and the compound phase $K_2Mg_2(SO_4)_3$, indicated as KM_2S_3 in the diagram, when it is cooled to the

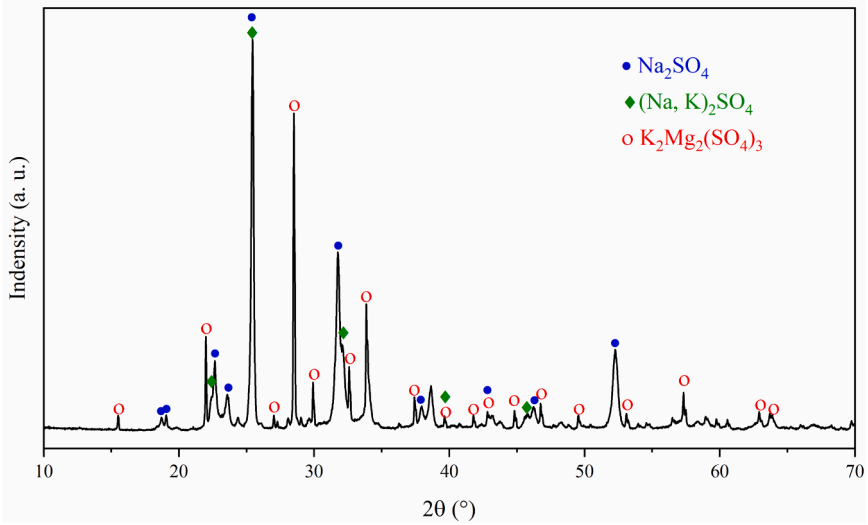

Fig. 7. XRD pattern of Na_2SO_4-$12K_2SO_4$-$35MgSO_4$ mixture (without NiAl-coated superalloy) after exposure at 700 °C for 24 h in air-300 ppm SO_2.

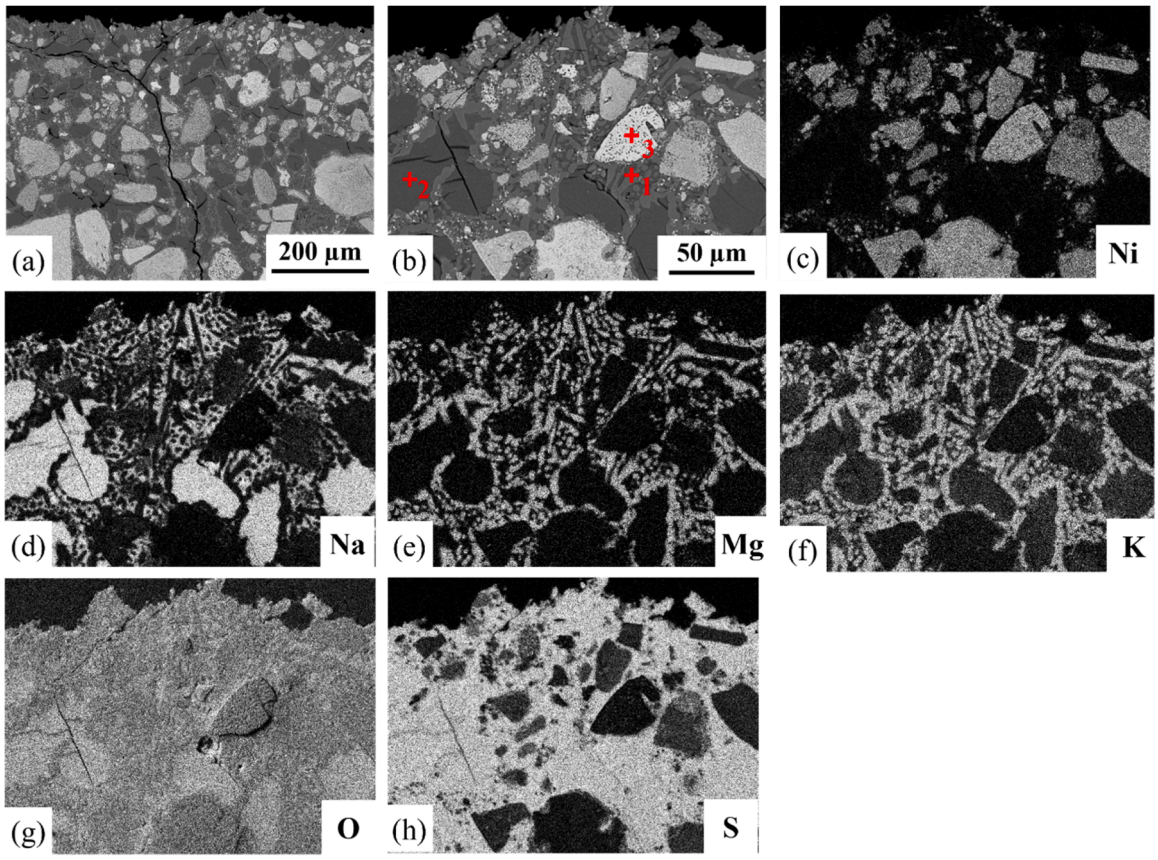

Fig. 8. (a)-(b) SEM-BSE image and (c)-(h) corresponding EDX-elemental maps of the cross-section of Na_2SO_4-7K_2SO_4-22$MgSO_4$-38NiO mixture (without NiAl-coated superalloy) after exposure at 700 °C for 100 h in air-300 ppm SO_2. Points designated 1–3 in (b) indicate locations of EDX point analyses and the corresponding results are summarized in Table 2.

Table 2
Chemical composition (at%) determined by EDX analysis at locations shown in Fig. 8.

Spectrum	O	S	Na	Mg	K	Ni
1	63.2	15.8	1.7	8.9	8.8	1.6
2	58.1	14.8	24.3	0.2	1.8	0.8
3	51.2	1.4	0.6	0.2	0.5	46.1

eutectic temperature 676 °C. As the cooling process continues, the HEXA phase transforms into another solid solution phase glaserite (designated as GLAS, [25,35,36]), which is a solid solution phase based on Na, K-sulphate. Another compound $Na_6Mg(SO_4)_4$ (N_3MS_4) is predicted to precipitate during cooling below approximately 460 °C. It can be seen more clearly from Fig. 11b that for a mixture of $K_2Mg_2(SO_4)_3$ and Na_2SO_4 with the content of Na_2SO_4 less than 76 mol.%, a liquid phase and the $K_2Mg_2(SO_4)_3$ compound phase can be expected at 700 °C in equilibrium condition. The solidification of the liquid phase upon cooling results in the formation of the HEXA phase, which transforms into the GLAS phase during cooling. At temperatures beneath approximately 470 °C, $Na_6Mg(SO_4)_4$ (indicated as N_3MS_4) is formed.

The calculations in Fig. 11 indicate that apart from $K_2Mg_2(SO_4)_3$ there exist other mixed compound sulphates between Na and Mg, namely $NaMg_3(SO_4)_4$ and $Na_6Mg(SO_4)_4$ designated as NM_3S_4 and N_3MS_4 in the diagrams. Formation of these phases might occur in the solid state and their existence might explain presence of minor peaks in the XRD-pattern in Fig. 7. However, it should be appreciated that the experimental microstructures might deviate from the calculated phase diagrams. The specimens were cooled down after the test within the furnace and the thermodynamic equilibrium at temperatures below 600°C might not have been reached in the experiments.

5. Discussion

5.1. *Effect of K_2SO_4 addition to Na_2SO_4 on the hot corrosion behaviour*

As shown in Fig. 1a after 24 h exposure of the studied NiAl coating under the Na_2SO_4 deposit only minor local pits containing mainly Al-rich mixed oxides were found [33]. Addition of 20 % K_2SO_4 to Na_2SO_4 resulted in a severe hot corrosion attack, and the corrosion products were identified to be Al-rich oxides intermixed with Ni oxide/sulphide bands. As discussed in detail in our previous work [33] the addition of K_2SO_4 to Na_2SO_4 reduced the melting temperature of the deposit as well the pSO_3 required to form the liquid phase upon contact of the deposit with NiO. The resulting rapid reaction was accompanied by formation of intermediate compounds: Na, K, Ni sulphate (cation ratio approximately 1:1:1) and, after 100 h exposure (Na, K)$_2$(Ni, Co)$(SO_4)_2$ (see Fig. 5). It was proposed [33] that formation of the latter compounds can further accelerate the corrosion reactions by tying up Ni.

5.2. *Formation of $K_2Mg_2(SO_4)_3$ and a liquid phase in the Na_2SO_4-K_2SO_4-$MgSO_4$ system*

Overlapping of K, Mg, S and O in the salt on top of the NiAl coated specimen after 24 h exposure at 700 °C in air plus 300 ppm SO_2 was recognised by the EDX analysis (Fig. 2), indicating the formation of a K, Mg-sulphate phase during the exposure. Considering the XRD result of the Na, K, Mg-sulphate powder mixture after 24 h exposure (Fig. 7), and the EDX analysis of the ternary sulphate salt-NiO mixture (Fig. 8, Fig. 9, Table 2), the K, Mg-sulphate phase found on top of the NiAl coating was

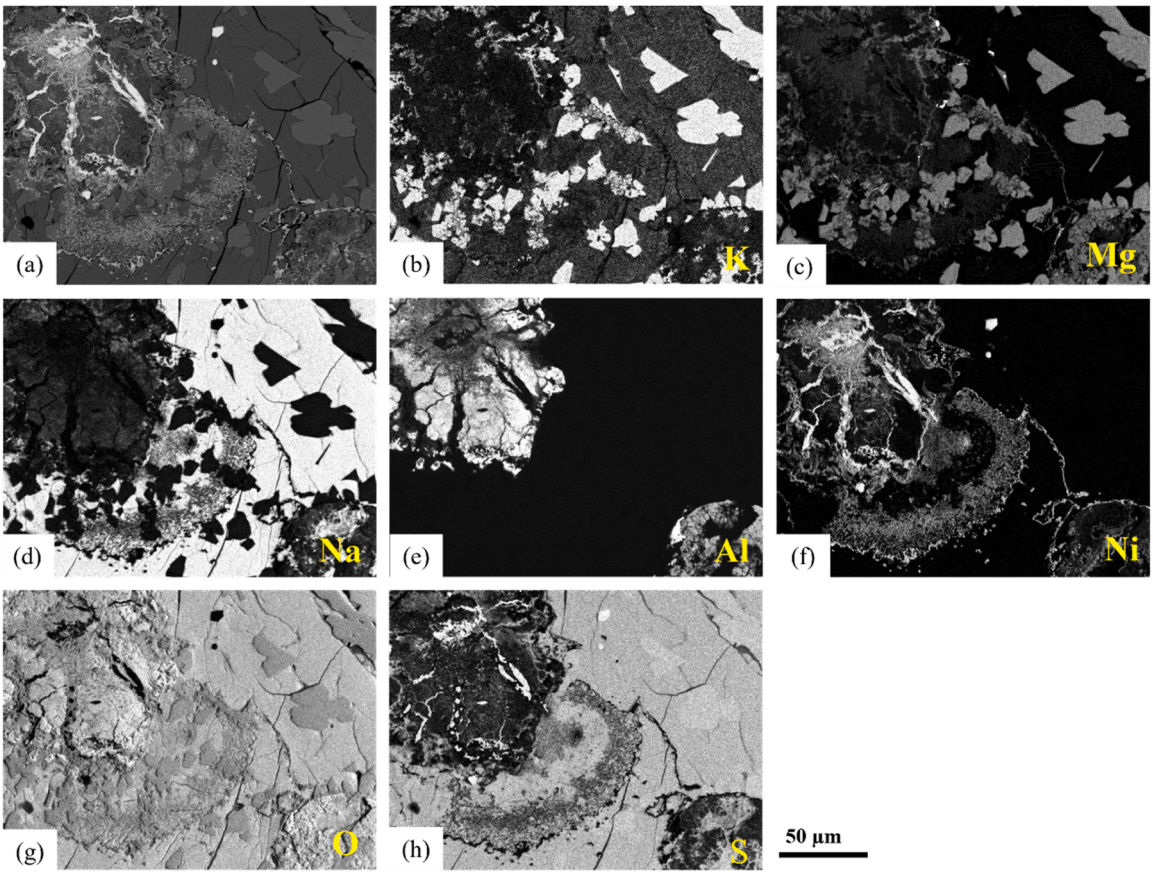

Fig. 9. (a) SEM-BSE image and (b)-(h) corresponding EDX-elemental maps of the cross-section of Na_2SO_4-7K_2SO_4-22$MgSO_4$-38NiAl mixture after exposure at 700 °C for 100 h in air-300 ppm SO_2.

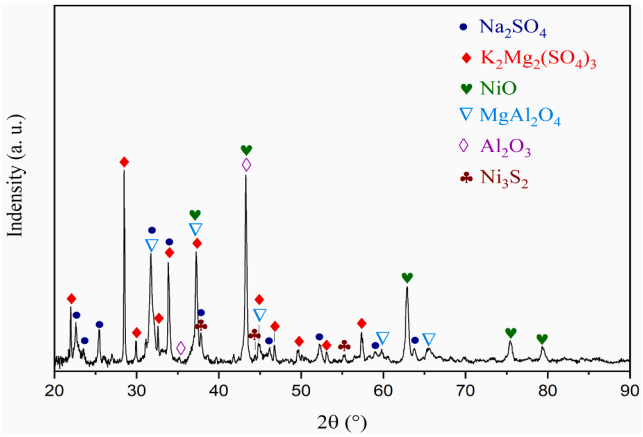

Fig. 10. XRD pattern of Na_2SO_4-7K_2SO_4-22$MgSO_4$-38NiAl powder mixture after exposure at 700 °C for 100 h in air-300 ppm SO_2.

identified to be a langbeinite compound with a formula $K_2Mg_2(SO_4)_3$. This compound was also identified on top of the NiAl coating (Fig. 6) and in the powder mixtures containing the ternary sulphate salt and NiO or NiAl (Fig. 8, Fig. 9, Table 2) after 100 h exposure. According to the K_2SO_4-$MgSO_4$ phase diagram [25], $K_2Mg_2(SO_4)_3$ is stable from room temperature up to 931 °C, above which it melts congruently. The most stable compound in the Na_2SO_4-$MgSO_4$ system is $Na_2Mg_3(SO_4)_4$ (melting temperature 813 °C [17,25]), and there is no stoichiometric intermediate compound in the Na_2SO_4-K_2SO_4 system. Therefore, $K_2Mg_2(SO_4)_3$ is the compound with the highest melting temperature among all known intermediate compounds in the studied ternary sulphate system.

According to the reported Na_2SO_4-K_2SO_4-$MgSO_4$ ternary phase diagram [24], and the calculated phase diagram of the pseudo-binary system $(MgSO_4)_{0.88}(K_2SO_4)_{0.12}$-$(Na_2SO_4)_{0.88}(K_2SO_4)_{0.12}$ (Fig. 11a), the solidus temperature of the Na_2SO_4-12K_2SO_4-35$MgSO_4$ mixture is 676 °C (the eutectic temperature). This means that the deposit contains a large fraction of liquid phase at the test temperature of 700 °C. This is in agreement with the morphology of the deposit shown in Fig. 2. During cooling after the exposure, the liquid phase solidified to form a solid solution Na_2SO_4 phase (HEXA or GLAS depending on the temperature, cooling rate, etc.) and $K_2Mg_2(SO_4)_3$. Phase diagrams in Fig. 11 indicate formation of mixed Na-Mg-sulphates according to solid state reactions. Formation of these phases could not be unequivocally proven by XRD due to insufficient time for the latter reactions to establish equilibrium during relatively fast cooling from the test temperature.

5.3. *The role of Mg in inhibiting the alkali sulphate induced hot corrosion*

Whereas the studied NiAl coated specimen was substantially corroded under the Na_2SO_4-20K_2SO_4 deposit after 24 hours exposure in air with 300 ppm SO_2 (Fig. 1a), virtually no corrosion attack was found in the specimen with addition of $MgSO_4$ to the alkali sulphate deposit after 24 hours (Fig. 1b). Apparently, the addition of $MgSO_4$ led to formation of the solid $K_2Mg_2(SO_4)_3$ phase, which effectively tied up K thereby preventing its adverse effect on the hot corrosion process described above.

Rahmel et al. [16] studied the effect of $MgSO_4$ addition on alkali sulphates induced hot corrosion of an austenitic Cr/Ni steel at 650 °C in air-20 % H_2O-(0.1–0.3)% SO_2, and found that the corrosion rate was considerably decreased with addition of more than 50 mol.% $MgSO_4$.

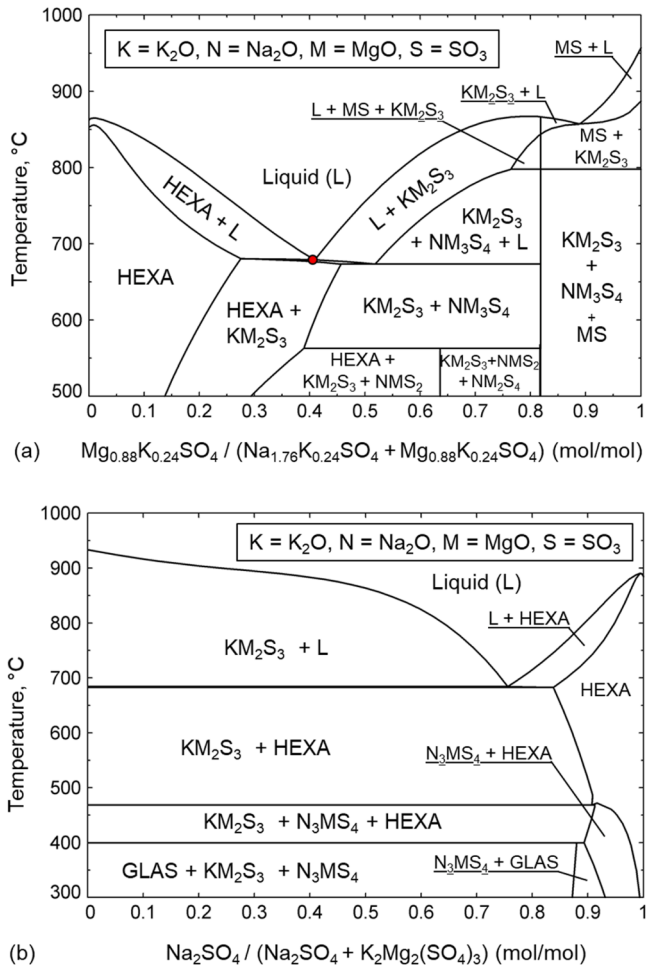

Fig. 11. Calculated phase diagrams of the pseudo-binary systems: (a) $(MgSO_4)_{0.88}(K_2SO_4)_{0.12}$-$(Na_2SO_4)_{0.88}(K_2SO_4)_{0.12}$; (b) $K_2Mg_2(SO_4)_3$-Na_2SO_4. HEXA and GLAS represent solid solution phases based on Na and K sulphates; The red point in (a) represents the eutectic point: Na_2SO_4-$12K_2SO_4$-$35MgSO_4$, 676 °C. For easier readability codes were used to indicate compositions of mixed sulphate compounds, e.g. $K_2Mg_2(SO_4)_3$ is designated as KM_2S_3. The coding system used is shown in framed inserts within diagrams.

The associated mechanism was proposed to be the formation of the thermodynamically very stable compound $K_2Mg_2(SO_4)_3$, which prevented hot corrosion reactions associated with the formation of $K_3Fe(SO_4)_3$. The latter mechanism is in qualitative agreement with the findings in the present work, whereas formation of Na,K,Ni-containing compounds was suppressed by formation of $K_2Mg_2(SO_4)_3$. In another study Rahmel and co-workers investigated [37] the hot corrosion behaviour of a series of Ni and Co based alloys with Na_2SO_4-$CaSO_4$-$MgSO_4$ salt at type I hot corrosion condition (at 900 °C) and concluded that due to the low stability of $MgSO_4$, the precipitation of a continuous MgO layer on the alloy surface would inhibit hot corrosion in basic conditions. Formation of MgO was not observed in the present work, likely due to the fact that the test temperature was significantly lower than that used in Rahmel's study [37].

An important observation in the present work was that no substantial corrosion with the Na_2SO_4-$12K_2SO_4$-$35MgSO_4$ deposit occurred after 24 h exposure in spite of an apparent formation of liquid phase. The liquid phase formation is supported by the thermodynamic calculations (Fig. 11) as well as by the morphologies of reacted deposit in Fig. 1b and Fig. 2. The latter morphology features a very dense matrix containing bulky, elongated $K_2Mg_2(SO_4)_3$ crystals, for which growth a fast diffusion transport prevailing in a liquid phase is required. Moreover, no substantial reaction was observed between the NiO powder and Na_2SO_4-$12K_2SO_4$-$35MgSO_4$ mixed powders even after 100 h exposure. After the latter experiment, the observed morphology of the reaction products also points to formation of a liquid phase during exposure at 700 °C (Fig. 8). These results indicate that the mere presence of a liquid phase is not sufficient to cause rapid hot corrosion. Ni-sulphation seems to be an important pre-requisite for the rapid attack, which apparently does not occur to a sufficient extent after exposure for 24 hours at 700 °C under the atmosphere with 300 ppm SO_2. It is noted that when the partial pressure of SO_2 in the atmosphere was increased to 1000 ppm, the coating reacted severely and substantial amounts of Ni-rich corrosion products were observed already after 24 hours (Fig. 3). The latter result stresses the importance of sufficiently high SO_3-activity in the melt for hot corrosion type II to occur.

5.4. *Acceleration of corrosion beneath ternary K-Na-Mg sulphate at longer exposure times*

During 100 h exposure in the atmosphere with a low SO_2 content (air - 300 ppm SO_2), the attack caused by the Na_2SO_4-$12K_2SO_4$-$35MgSO_4$ mixture is as severe as that caused by the Na_2SO_4-$20K_2SO_4$ mixture (Fig. 4). In other words: the inhibitive effect of Mg found after 24 h is lost after longer time exposure. Elucidating the corrosion mechanism responsible for this effect is difficult when analysing the corrosion products in the coated superalloy due to the presence of alloying elements within the coating (Cr, Co) and the interdiffusion zone (Re, W). For deriving the corrosion mechanisms, analysis of the reacted Na_2SO_4-$12K_2SO_4$-$35MgSO_4$-NiAl powder mixtures appears to be more suitable. According to the XRD-pattern in Fig. 10, several reaction products are identified, including NiO, Ni_3S_2, Al_2O_3 and a spinel phase. The reaction of the NiAl powder with the salt mixture is far more severe compared to that of the NiO powder (compare Fig. 8 and Fig. 9). This finding indicates the importance of reactions between the salt mixture and Al for the mechanism of accelerated corrosion.

Fig. 12 shows a phase map produced by "superimposing" the EDX-maps in Fig. 9 to illustrate distribution of the various phases for the case of Na_2SO_4-$7K_2SO_4$-$22MgSO_4$-38NiAl powder mixture after exposure at 700 °C in air-300 ppm SO_2 for 100 h. In the upper right part of the map the two-phase microstructure of the deposit not affected by reaction with the NiAl powder can be seen consisting of Na_2SO_4 (Na-S-O) and large (30–50 μm in size) $K_2Mg_2(SO_4)_3$ crystals (K-Mg-S-O). In the upper left part of the map a reacted NiAl powder particle can be observed. This particle consists mainly of alumina (Al-O) along with a Mg, Ni and Al containing mixed oxide, likely a spinel (Mg-Ni-Al-O), Ni-rich oxide (Ni-Mg-S-O) and Ni-sulphide (Ni-S). In the middle and bottom left part of the map further reaction products can be seen namely Na_2SO_4 with dissolved Ni (Na-Ni-S-O). According to the respective EDX map, the latter region contains some K. It is important to mention that the size and distribution of the $K_2Mg_2(SO_4)_3$ crystals is changed in the vicinity of the reacted NiAl-particle in agreement with partitioning of Mg into (Mg, Ni)Al_2O_4. The phases, which can be identified by the EDX maps in Fig. 12 are in good agreement with the XRD-results in Fig. 10.

Based on the obtained results it is very likely that the loss of the inhibitive effect of Mg on the corrosion of the NiAl coating in the ternary Na-K-Mg sulphate deposit after extended exposure time (here 100 h) is related to reactions involving Al. The exact mechanism might include formation of a spinel phase of the (Mg,Ni)Al_2O_4 type causing dissociation of $K_2Mg_2(SO_4)_3$ and consequently release of potassium ions. The released potassium might accelerate the corrosion rate by lowering the minimum p_{SO3} required for the Ni-sulphation as mentioned above and shown in our previous study [33]. However, this mechanism alone cannot explain why the reaction acceleration occurs somewhere between 24 and 100 h exposure and not at earlier time in spite of the apparent presence of liquid phase before 24 h. Therefore, the exact corrosion mechanism might be more complex involving incorporation of SO_3 possibly transformed into $S_2O_7^{2-}$ into the liquid phase, its diffusion to the NiAl-coating surface and reaction to produce alumina, Ni-oxide and

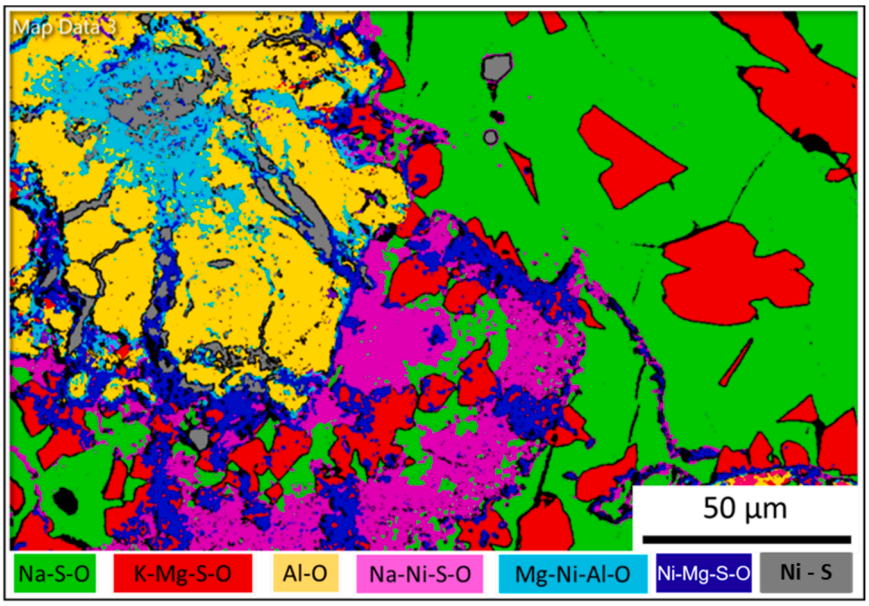

Fig. 12. Phase map of Na_2SO_4-7K_2SO_4-22$MgSO_4$-38NiAl powder mixture cross-section after exposure at 700 °C for 100 h in air-300 ppm SO_2 (compare with Fg.9). See the text for explanations.

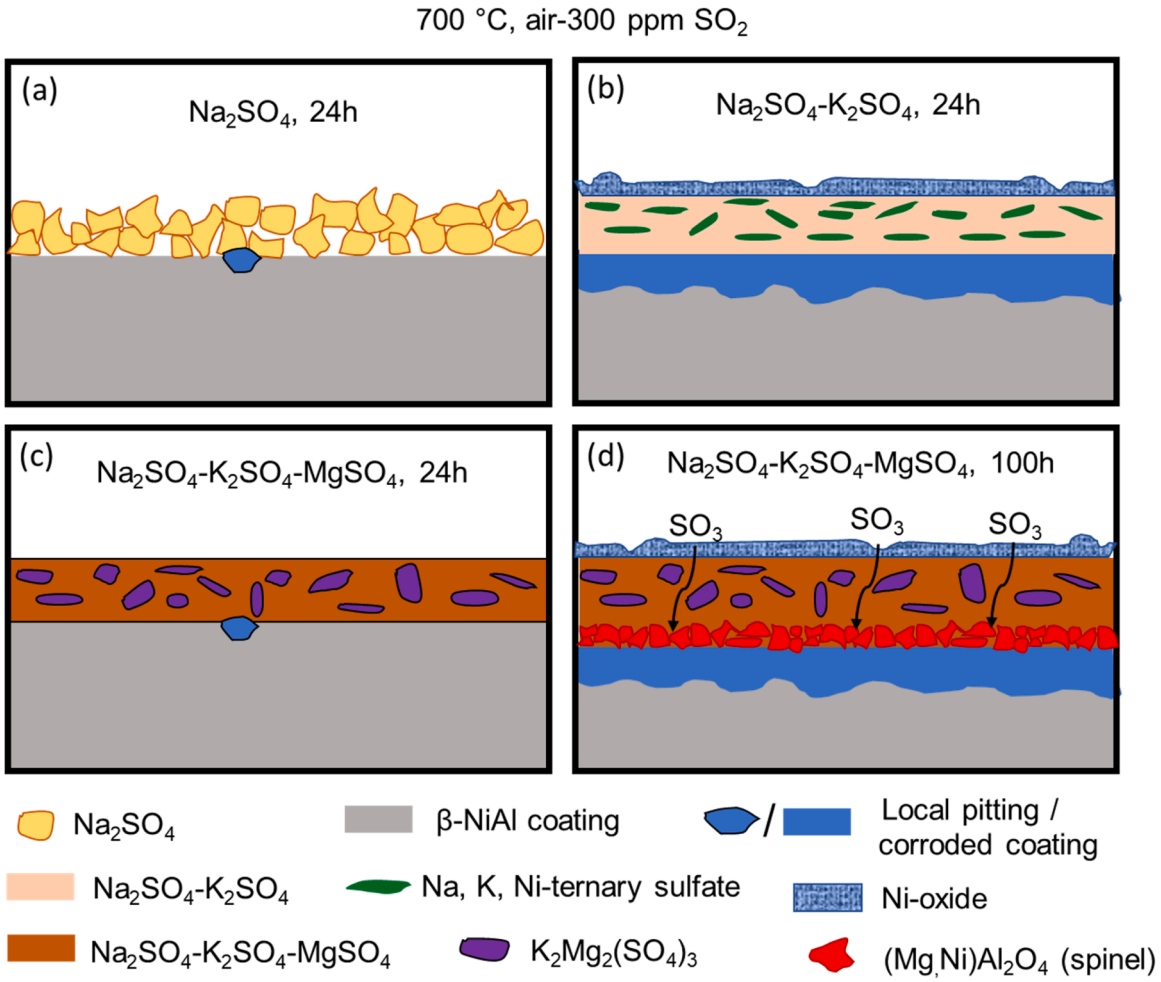

Fig. 13. Schematic illustrating the mechanisms of hot corrosion reactions of the studied NiAl-coating: a), b) after exposure for 24 hours under Na_2SO_4 and Na_2SO_4-K_2SO_4 deposits, respectively; and c), d) under Na_2SO_4-K_2SO_4-$MgSO_4$ deposit after exposure for 24 hours and 100 hours, respectively. Minor internal chromium sulfidation in the coating below the corrosion front is neglected for simplicity. See the text for explanations.

eventually (Mg,Ni)Al_2O_4. The diffusion of the oxidant through the melt might explain delayed propagation stage of hot corrosion. Thus, formation of the spinel is an important preceding step for Ni-sulphation under the particularly studied ternary Na-K-Mg-sulphate deposit.

The various mechanisms of the hot corrosion reactions under the studied deposit compositions at 700 °C in a 300 ppm SO_2 containing synthetic air based test gas are illustrated schematically in Fig. 13. Under the unary Na_2SO_4 deposit only minor local corrosion is observed after 24 hours (Fig. 13a) because there is hardly any liquid sulfate formation under the prevailing test condition [33]. Addition of K_2SO_4 to the Na_2SO_4 deposit produces a liquid phase in contact with the coating and a rapid corrosion occurs combined with the formation of a Na, K, Ni ternary sulfate (Fig. 13b). Under the Na-K-Mg-sulphate the NiAl-coating exhibits initially, i.e. after 24 hours exposure, only minor local corrosion (Fig. 13c). At this stage K is to a large extent tied up in the $K_2Mg_2(SO_4)_3$ solid compound, which prevents its deleterious effect on the corrosion of the Na_2SO_4-based deposit. However, at longer exposure times diffusion of SO_3 through the melt results in a reaction of the NiAl-coating into alumina and Ni-oxide, whereas subsequent formation of Mg, Ni and Al containing spinel leads to release of K causing accelerated corrosion (Fig. 13 d).

The results of the present work indicate that the effect of $MgSO_4$ addition to the base salt mixture (Na_2SO_4 and/or K_2SO_4) on the hot corrosion behaviour of the Ni-base alloys and coatings will not only depend on time, temperature and SO_2 content in the gas. The effect may be very different depending on the exact chemical composition of the actual material, in particular on its Al-content. Future work on correlation between the alloy and deposit chemistry and the corrosion behaviour could benefit from thermodynamic equilibria calculations with optimized databases by incorporating data for various Na, K, Mg, Ni and Al containing oxide, sulphide and sulphate phases.

6. Conclusions

In our previous study [33] it was shown that addition of K_2SO_4 to a Na_2SO_4 based deposit strongly enhanced the type II hot corrosion attack of a β-NiAl coating on a Ni-base superalloy during exposure at 700 °C in dry synthetic air with 300 ppm SO_2. For elucidating a possible effect of $MgSO_4$ addition to the alkali sulphate deposit on the corrosion attack, the present work studied the behaviour of the same coating system under Na_2SO_4-12K_2SO_4-35$MgSO_4$ deposit mixture. A series of tests were performed at 700 °C in dry synthetic air with 300 and 1000 ppm SO_2. For obtaining a more detailed understanding of the corrosion mechanisms mixtures of sulphate salts and NiO or NiAl, powders were exposed under the same conditions as the aluminized alloy specimens. Thermodynamic assessment of the Na-K-Mg sulfate deposit was performed using FactSage and an in-house developed thermodynamic database. Based on the obtained experimental and modelling results the following conclusions can be drawn:

1. After 24 and 100 h exposure at 700 °C in dry synthetic air with 300 ppm SO_2, an intermediate compound $K_2Mg_2(SO_4)_3$ was found in the Na_2SO_4-12K_2SO_4-35$MgSO_4$ powder mixture (with or without NiO/NiAl) as well as in the deposit present on the NiAl coating.
2. Formation of the $K_2Mg_2(SO_4)_3$ compound inhibited the hot corrosion attack of the studied NiAl coating observed in the case of a binary Na_2SO_4-20K_2SO_4 mixture during the 24 h exposure. The suppression of rapid hot corrosion occurred in spite of apparent formation of liquid phase. The inhibition effect of $MgSO_4$ is very likely related to the consumption of the aggressive alkali deposit component K_2SO_4.
3. Extending the exposure time of the studied NiAl coating with Na_2SO_4-12K_2SO_4-35$MgSO_4$ mixture at 700 °C in air-300 ppm SO_2 to 100 h resulted in a severe hot corrosion attack, i.e. similar to that in the Mg-free salt mixture. Based on the prevailing experimental results formation of Al-rich oxides (in particular Mg, Ni and Al containing spinel) is believed to be an important reaction step destabilizing the $K_2Mg_2(SO_4)_3$ compound, thereby releasing K-sulfate, which initiates the accelerated corrosion. The finding in the present study regarding a possible significant effect of $MgSO_4$ seems to be (partly) different from the results of some other authors [16, 21–23]. Based on the mechanism discussed here, this seems not necessarily to be a contradiction.
4. The mechanisms derived in the present work indicate that the effect of $MgSO_4$ addition to the base salt mixture (Na_2SO_4 and/or K_2SO_4) on the hot corrosion behaviour of the Ni-base alloys and coatings will not only depend on the exact salt chemistry, temperature and SO_2-content in the gas phase. It may differ depending on the detailed chemical composition of the actual alloy or coating system.

Author statement

I the undersigned declare that this manuscript is original, has not been published before and is not currently being considered for publication elsewhere. I confirm that the manuscript has been read and approved by all named authors and that there are no other persons who satisfied the criteria for authorship but are not listed. I further confirm that the order of authors listed in the manuscript has been approved by the other authors. The other authors understand that the Corresponding Author is the sole contact for the Editorial process responsible for communicating with the other authors about progress, submissions of revisions and final approval of proofs.

CRediT authorship contribution statement

Grüner Daniel: Investigation. **Wessel Egbert:** Investigation. **Wang Yaping:** Conceptualization, Investigation, Methodology, Writing – original draft. **Naumenko Dmitry:** Conceptualization, Project administration, Resources, Supervision, Writing – original draft, Writing – review & editing. **Quadakkers Willem J:** Conceptualization, Methodology, Resources, Writing – review & editing. **Müller Michael:** Resources, Supervision, Writing – review & editing. **Frommherz Martin:** Funding acquisition, Project administration, Validation, Writing – review & editing. **Yazhenskikh Elena:** Data curation, Writing – review & editing. **Pillai Rishi:** Conceptualization, Funding acquisition, Supervision, Validation.

Declaration of Competing Interest

The authors declare that they have no known competing financial interests or personal relationships that could have appeared to influence the work reported in this paper.

Acknowledgements

Mr. H. Cosler is kindly acknowledged for performing the hot corrosion tests. The authors are grateful to Mr. M. Ziegner for the XRD analysis. The authors thank China Scholarship Council (No. 201708440229) for the financial support. Part of the work was supported by Federal Ministry of Economic Affairs and Energy and MTU Aero Engines AG (Grant numbers: 20T1522A, 20T1302A).

Data availability

Data will be made available on request.

References

[1] J. Sumner, A. Encinas-Oropesa, N.J. Simms, et al., Type II hot corrosion: kinetics studies of CMSX-4, Oxid. Met. 80 (5-6) (2013) 553–563, https://doi.org/10.1007/s11085-013-9395-x.
[2] A.U. Syed, F.D. Martinez, T. Roberts, et al., Performance comparison between isothermal hot corrosion and in situ cyclic hot corrosion of nickel-based

superalloys, Oxid. Met. 96 (1-2) (2021) 43–55, https://doi.org/10.1007/s11085-021-10044-9.
[3] J.A. Goebel, F.S. Pettit, G.W. Goward, Mechanisms for the hot corrosion of nickel-base alloys, Metall. Trans. 4 (1973) 261–279, https://doi.org/10.1007/BF02649626.
[4] K.L. Luthra, Low temperature hot corrosion of cobalt-base alloys: part II. reaction mechanism, Metall. Trans. A 13A (1982) 1853–1864, https://doi.org/10.1007/BF02647842.
[5] A.K. Misra, D.P. Whittle, W.L. Worrell, Thermodynamics of molten sulfate mixtures, J. Electrochem. Soc. 129 (1982) 1840–1845, https://doi.org/10.1149/1.2124305.
[6] Y.-S. Hwang, R.A. Rapp, Synergistic dissolution of oxides in molten sodium sulfate, J. Electrochem. Soc. 137 (4) (1990) 1276–1280, https://doi.org/10.1149/1.2086647.
[7] J.M. Alvarado-Orozco, J.E. Garcia-Herrera, B. Gleeson, et al., Reinterpretation of type II hot corrosion of Co-base alloys incorporating synergistic fluxing, Oxid. Met. 90 (5-6) (2018) 527–553, https://doi.org/10.1007/s11085-018-9853-6.
[8] E. Kistler, W.-T. Chen, G.H. Meier, et al., A new solid-state mode of hot corrosion at temperatures below 700 °C, Mater. Corros. 70 (8) (2019) 1346–1359, https://doi.org/10.1002/maco.201810751.
[9] T. Gheno, M. Zahiri Azar, A.H. Heuer, et al., Reaction morphologies developed by nickel aluminides in type II hot corrosion conditions: The effect of chromium, Corros. Sci. 101 (2015) 32–46, https://doi.org/10.1016/j.corsci.2015.08.029.
[10] A.K. Misra, D.P. Whittle, Effects of SO_2 and SO_3 on the Na_2SO_4 induced corrosion of nickel, Oxid. Met. 22 (1984) 1–33, https://doi.org/10.1007/BF00659246.
[11] N.S. Bornstein, Reviewing sulfidation corrosion-Yesterday and today, JOM 48 (11) (1996) 37–39, https://doi.org/10.1007/bf03223242.
[12] D.A. Shifler. The increasing complexity of hot corrosion. in ASME Turbo Expo: Turbomachinery Technical Conference and Exposition GT. 2017. DOI: ⟨10.1115/GT2017-65281⟩.
[13] W. Braue, Environmental stability of the YSZ layer and the YSZ/TGO interface of an in-service EB-PVD coated high-pressure turbine blade, J. Mater. Sci. 44 (7) (2009) 1664–1675, https://doi.org/10.1007/s10853-008-3215-8.
[14] G.H. Meier, Invited review paper in commemoration of over 50 years of oxidation of metals: Current aspects of deposit-induced corrosion, Oxid. Met. (2021), https://doi.org/10.1007/s11085-020-10015-6.
[15] N. Bornstein, W. Allen, The chemistry of sulfidation corrosion-revisited. Materials Science Forum, Trans Tech Publications, 1997, pp. 127–134, https://doi.org/10.4028/www.scientific.net/MSF.251-254.127.
[16] A. Rahmel, Influence of calcium and magnesium sulfates on the high temperature oxidation of Austenitic chrome-nickel steels in the presence of alkali sulfate and sulfur trioxides, Mech. Corros. Fuel Impurities (1963) 556.
[17] R. Nacken, Ueber Langbeinit und Vanthoffit (K_2SO_4•$2MgSO_4$ und $3Na_2SO_4$•$MgSO_4$), Nachr. Von. der Ges. der Wiss. zu Göttingen, Math. -Phys. Kl. 1907 (1907) 602–613.
[18] S.M. Mukimov, Z.I. Filippova, Reactions in melts of Na, K, Mg, and Ca sulfates, Tr. Inst. Khim., Akad. Nauk Uzb. S. S. S. R., Inst. Khim. 2 (1949) 123–132.
[19] J.J. Rowe, G.W. Morey, C.C. Silber, The ternary system K_2SO_4-$MgSO_4$-$CaSO_4$, J. Inorg. Nucl. Chem. 29 (4) (1967) 925–942, https://doi.org/10.1016/0022-1902(67)80075-7.
[20] J.J. Rowe, G.W. Morey, I.D. Hansen, The binary system K_2SO_4-$CaSO_4$, J. Inorg. Nucl. Chem. 27 (1) (1965) 53–58, https://doi.org/10.1016/0022-1902(65)80189-0.
[21] R.L. Jones, C.E. Williams, Mixed $MgSO_4$-Na_2SO_4 effects in the 973 K hot corrosion of CoCrAlY, J. Electrochem. Soc. 133 (1) (1986) 217–223, https://doi.org/10.1149/1.2108527.
[22] T. König, X. Montero, M. Galetz, The influence of iron and cobalt on the type II hot corrosion behavior of NiCr model alloys, Mater. Corros. 71 (7) (2020) 1138–1151, https://doi.org/10.1002/maco.201911376.
[23] X. Montero, A. Ishida, T.M. Meißner, et al., Effect of surface treatment and crystal orientation on hot corrosion of a Ni-based single-crystal superalloy, Corros. Sci. 166 (2020), https://doi.org/10.1016/j.corsci.2020.108472.
[24] E. Yazhenskikh, T. Jantzen, Y. Wang, et al., Thermodynamic description of the ternary systems of the core sulphate system Na_2SO_4-K_2SO_4-$MgSO_4$-$CaSO_4$, Calphad 74 (2021) 102313, https://doi.org/10.1016/j.calphad.2021.102313.
[25] E. Yazhenskikh, T. Jantzen, D. Kobertz, et al., Critical thermodynamic evaluation of the binary sub-systems of the core sulphate system Na_2SO_4-K_2SO_4-$MgSO_4$-$CaSO_4$, Calphad 72 (2021) 122234, https://doi.org/10.1016/j.calphad.2020.102234.
[26] E. Yazhenskikh, T. Jantzen, K. Hack, et al., A new multipurpose thermodynamic database for oxide systems, РАСПЛАВЫ (Melts) (2) (2019) 116–124, https://doi.org/10.1134/s0235010619010237.
[27] R. Pillai, A. Chyrkin, D. Grüner, et al., Carbides in an aluminised single crystal superalloy: tracing the source of carbon, Surf. Coat. Technol. 288 (2016) 15–24, https://doi.org/10.1016/j.surfcoat.2015.12.066.
[28] E. Jänecke, Über das Schmelz-und Erstarrungsbild des doppelt-ternären Systemes (K_2· Na_2· Mg)(Cl_2· SO_4), Z. F. üR. Anorg. Chem. 261 (3-4) (1950) 213–225.
[29] A. Bellanca, P. di Mineralogia, L'aftitalite nel sistema ternario K_2SO_4-Na_2SO_4-$CaSO_4$, Period. di Mineral. 13 (1942) 21–86.
[30] J.A. O'Brien, J.T. Hinkley, S.W. Donne, Electrochemical oxidation of aqueous sulfur dioxide II. Comparative studies on platinum and gold electrodes, J. Electrochem. Soc. 159 (9) (2012) F585–F593, https://doi.org/10.1149/2.060209jes.
[31] K.L. Luthra, Low temperature hot corrosion of cobalt-base alloys: part I. Morphology of the reaction product, Metall. Trans. A 13A (1982) 1843–1852, https://doi.org/10.1007/BF02647841.
[32] M. Hellenbrandt, The inorganic crystal structure database (ICSD)-Present and future, Crystallogr. Rev. 10 (1) (2004) 17–22, https://doi.org/10.1080/08893110410001664882.
[33] Y. Wang, R. Pillai, E. Yazhenskikh, et al., Comparison of Na2SO4, K2SO4 and Na2SO4-K2SO4 deposit induced hot corrosion of a β-NiAl coating. 2022. 198: 110146. DOI: ⟨10.1016/j.corsci.2022.110146⟩.
[34] C.W. Bale, E. Bélisle, P. Chartrand, et al., FactSage thermochemical software and databases, 2010–2016, Calphad 54 (2016) 35–53, https://doi.org/10.1016/j.calphad.2016.05.002.
[35] H. Du, Thermodynamic assessment of the K_2SO_4-Na_2SO_4-$MgSO_4$-$CaSO_4$ system, J. Phase Equilibria 21 (1) (2000) 6–18, https://doi.org/10.1361/105497100770340363.
[36] D. Lindberg, R. Backman, P. Chartrand, Thermodynamic evaluation and optimization of the (Na_2SO_4+K_2SO_4+$Na_2S_2O_7$+$K_2S_2O_7$) system, J. Chem. Thermodyn. 38 (12) (2006) 1568–1583, https://doi.org/10.1016/j.jct.2006.04.002.
[37] M.S.A. Rahmel, Monika Schorr, The influence of electrode potential on the corrosion ot gas turbine alloys in sulfate melts, Oxid. Met. 18 (3) (1982) 195–223, https://doi.org/10.1007/BF00662038.